Da Silva, Alejandro J., Hästbacka, Hendrik S. E., Luoto, Jens C., Gough, Rosemarie E., Coelho-Rato, Leila S., Laitala, Leena M., Goult, Benjamin T, Imanishi, Susumu Y., Sistonen, Lea and Henriksson, Eva (2024) *Proteomic profiling identifies a direct interaction between heat shock transcription factor 2 and the focal adhesion adapter talin-1.* The FEBS Journal, 291 (21). pp. 4830-4848. ISSN 1742-464X.

Proteomic profiling identifies a direct interaction between heat shock transcription factor 2 and the focal adhesion adapter talin-1

Alejandro J. Da Silva[1,2] (iD), Hendrik S. E. Hästbacka[1,2] (iD), Jens C. Luoto[1,2] (iD),
Rosemarie E. Gough[3], Leila S. Coelho-Rato[1,2], Leena M. Laitala[1,2], Benjamin T. Goult[3,*] (iD),
Susumu Y. Imanishi[4], Lea Sistonen[1,2] (iD) and Eva Henriksson[1,2] (iD)

1 Faculty of Science and Engineering, Cell Biology, Åbo Akademi University, Turku, Finland
2 Turku Bioscience Centre, University of Turku and Åbo Akademi University, Turku, Finland
3 School of Biosciences, University of Kent, Canterbury, UK
4 Faculty of Pharmacy, Meijo University, Nagoya, Japan

Heat shock factor 2 (HSF2) is a versatile transcription factor that regulates gene expression under stress conditions, during development, and in disease. Despite recent advances in characterizing HSF2-dependent target genes, little is known about the protein networks associated with this transcription factor. In this study, we performed co-immunoprecipitation coupled with mass spectrometry analysis to identify the HSF2 interactome in mouse testes, where HSF2 is required for normal sperm development. Endogenous HSF2 was discovered to form a complex with several adhesion-associated proteins, a finding substantiated by mass spectrometry analysis conducted in human prostate carcinoma PC-3 cells. Notably, this group of proteins included the focal adhesion adapter protein talin-1 (TLN1). Through co-immunoprecipitation and proximity ligation assays, we demonstrate the conservation of the HSF2-TLN1 interaction from mouse to human. Additionally, employing sequence alignment analyses, we uncovered a TLN1-binding motif in the HSF2 C terminus that binds directly to multiple regions of TLN1 *in vitro*. We provide evidence that the 25 C-terminal amino acids of HSF2, fused to EGFP, are sufficient to establish a protein complex with TLN1 and modify cell–cell adhesion in human cells. Importantly, this TLN1-binding motif is absent in the C-terminus of a closely related HSF family member, HSF1, which does not

Abbreviations

ACRBP, acrosin binding protein; AD, transactivation domain; BSA, bovine serum albumin; CBP/EP300, CREB-binding protein/E1A binding protein P300; ChIP-chip, chromatin immunoprecipitation coupled to microarray hybridization; ChIP-seq, chromatin immunoprecipitation sequencing; co-IP, co-immunoprecipitation; CTNND, catenin delta; DAPI, 4′,6-diamidino-2-phenylindole; DBD, DNA-binding domain; DD, dimerization domain; DIA, data-independent acquisition; DTT, dithiothreitol; EDTA, ethylenediaminetetraacetic acid; EGF, epidermal growth factor; FBS, fetal bovine serum; FN, fibronectin; GO, gene ontology; GOGA, golgin subfamily A member; HEPES, (4-(2-hydroxyethyl)-1-piperazineethanesulfonic acid); HPLC, high-performance liquid chromatography; HR, heptad repeat; HSF, heat shock factor; HSP, heat shock protein; HSPA, heat shock protein family A member; IgG, immunoglobulin G; KANK, kidney or KN motif and ankyrin repeat domain-containing; LC-ESI-MS/MS, liquid chromatography-electrospray ionization-mass spectrometry; LC–MS/MS, liquid chromatography tandem mass spectrometry; MAP, microtubule-associated protein; mEGFP, monomeric enhanced green fluorescent protein; MSH, DNA mismatch repair protein; Nek, never in mitosis gene A (NIMA) related kinase; NPHP, nephrocystin; PBS, phosphate-buffered saline; PC-3, prostate cancer cells; PFA, paraformaldehyde; PLA, proximity ligation assay; PMSF, phenylmethylsulfonyl fluoride; PSM, peptide spectrum matches; PXN, paxillin; RD, regulatory domain; RIAM, Rap1-interacting adaptor molecule; SAINT, significance analysis of interactome; SEM, standard error of the mean; shRNA, short hairpin RNA; SMC, structural maintenance of chromosomes; SYCP, synaptonemal complex protein; TCEP, tris(2-carboxyethyl)phosphine; TLN, talin; TOP2A, DNA topoisomerase II alpha; ULA, ultra-low attachment; ZO, zonula occludens.

form a complex with TLN1. These results highlight the unique molecular characteristics of HSF2 in comparison to HSF1. Taken together, our data unveil the protein partners associated with HSF2 in a physiologically relevant context and identifies TLN1 as the first adhesion-related HSF2-interacting partner.

Introduction

All living organisms must respond effectively to environmental insults that challenge the homeostasis of their proteome. For this purpose, every kingdom of life possesses a stress response mechanism known as the heat shock response, which involves the expression of molecular chaperones called heat shock proteins (HSPs) [1]. The expression of HSPs is regulated by a family of transcription factors known as heat shock factors (HSFs), of which HSF1 and HSF2 are the most studied members in mammals [2]. While HSF1 is indispensable in response to acute proteotoxic stress, HSF2 cooperates with HSF1 to drive gene expression under adverse conditions [3–5]. Intriguingly, HSF2 is essential for cell survival upon chronic accumulation of misfolded proteins, which shows the independent role of this transcription factor in cellular stress responses [6–8].

In addition to stress, HSF1 and HSF2 play important roles in physiological processes, such as embryogenesis, corticogenesis, and spermatogenesis [2,9]. Among adult tissues, testes possess the highest levels of HSF2 protein [10,11]. Interestingly, mice lacking HSF2 are characterized by reduced testes size, a disorganized structure of seminiferous tubules, pronounced apoptosis in the pachytene spermatocytes, and defects in the quality and number of sperm [12–14]. Moreover, mice lacking both HSF1 and HSF2 suffer from a severe disruption of spermatogenesis leading to male infertility [15]. Thus, there is accumulating evidence that HSF1 and HSF2 act synergistically during spermatogenesis, which is congruent with ChIP-chip and ChIP-seq experiments showing co-occupancy of genomic loci of these HSFs in mouse testes [14,16,17].

In contrast to the knowledge of downstream targets of HSF1 and HSF2 in stress and development [2,9,12], little is known about the protein networks that are associated with these HSFs in different biological contexts. A recent study approached this gap in knowledge by screening for HSF1-binding partners under control conditions, in comparison to responses to either acute (heat shock) or chronic (Huntington's disease) proteotoxic stress [18]. However, no similar unbiased investigations have been reported for HSF2. Currently, the best-characterized HSF2-binding partner is HSF1, since a wealth of studies have provided a deep understanding of the HSF1-HSF2 protein complex [19–22]. HSF1 and HSF2 form homo- and heterotrimers through their highly homologous oligomerization domains, which are composed of two leucine-zipper-like heptad repeats (HR-A and HR-B) [23]. Apart from HSF1, only a handful of HSF2-interacting partners have been previously reported and validated, including the molecular chaperone HSP90 [24], members of the E3 ubiquitin ligase anaphase/cyclosome protein complex [25], a subunit of a cullin-RING E3 ubiquitin ligase cullin 3 [26], small ubiquitin-related modifier 1 [27], and the acetyltransferase CBP/EP300 [28].

In this study, we investigated the interactome of endogenous HSF2 in mouse testes and human prostate carcinoma PC-3 cells. Our data shows that HSF2 interacts with several adhesion-associated proteins, i.e. FN1, TLN1, ZO1, and ZO2. Of these proteins, we focused on the mechanosensitive focal adhesion adapter protein talin-1 (TLN). TLN1 plays a fundamental role in the formation of cell-matrix adhesion by connecting integrin transmembrane receptors to the actin cytoskeleton [29,30]. TLN1 functions as an adapter and several TLN1-binding motifs have been well-characterized in different proteins [31]. Intriguingly, we found a TLN1-binding motif at the C-terminus of HSF2, which is absent in HSF1. By performing a fluorescent polarization assay, we found that this binding motif in HSF2 binds directly with multiple regions of TLN1. We demonstrate that the HSF2-TLN1 interaction is conserved from mouse to human and that the 25 C-terminal amino acids of HSF2 are sufficient to form a protein complex with TLN1 in human cells and affect cell–cell adhesion. In summary, our study presents the first HSF2 interactome in a physiological context, identifying TLN1, the focal adhesion adapter protein, as a novel HSF2-specific interacting partner.

Results

Identification of HSF2-binding partners in mouse testes

To identify proteins interacting with endogenous HSF2 *in vivo*, we performed an HSF2 co-immunoprecipitation (co-IP) coupled with liquid chromatography–tandem mass spectrometry (LC–MS/MS) from mouse testes (Fig. 1A). Mouse testes were used because we and others have shown that the protein levels of HSF2 are exceptionally high in this tissue, and lack of HSF2 disrupts the process of spermatogenesis [10,12,14,15]. HSF2 was immunoprecipitated with an HSF2-specific antibody and IgG was used as a negative control. Immunoblotting of the HSF2 co-IP sample showed that HSF2 was efficiently enriched as compared to the IgG and input controls (Fig. 1B). Additionally, we validated the formation of HSF2-HSF1 protein complexes in the co-IP sample, since these transcription factors have been shown to associate in mouse testes [21]. Once the quality of the co-IP samples was verified, the HSF2 interactome was determined through LC–MS/MS. This MS analysis identified 464 proteins in the HSF2 co-IP sample, and 461 in the IgG control (Fig. 1C, Table S1). Of these proteins, we chose the high-confidence HSF2-binding partners (proteins with at least two peptide spectrum matches [PSMs] and a ratio of HSF2 PSMs/IgG PSMs > 3), which led to the identification of 105 HSF2 partners. Notably, the MS analysis identified proteins involved in sperm morphogenesis (MAP7, NPHP1), sperm-egg recognition (ACRBP, HSPA2), and meiosis (GOGA3, Nek1, SYCP1), which is congruent with the role of HSF2 in spermatogenesis.

To gain more insights into the type of proteins that were enriched among the 105 HSF2-binding partners, we performed a gene ontology (GO) term analysis with the online tool SHINYGO [32] (Fig. 1D). Surprisingly, cell adhesion molecule binding was the predominant GO term (Fig. 1D,E). This is particularly interesting because previous studies have shown that lack of HSF2 alters the expression of cell adhesion-related genes, even though no proteins involved in cell adhesion have been validated as HSF2-binding partners [6,33]. The unfolded protein binding GO term was also highly enriched, wherein several proteins belonging to the HSP70 and HSP90 chaperone families were found (Fig. 1E). This is in agreement with a recent report showing an interaction between HSF2 and HSP90 [24].

Next, we validated proteins from the HSF2 interactome through co-IP using lysates from mouse testes (Fig. 1F). Since HSF2 is a transcription factor that binds to specific sequences of DNA [23], we selected the following chromatin-associated proteins MutS homolog 2 (MSH2) [34], structural maintenance of chromosome 2 (SMC2) [35], DNA topoisomerase 2-alpha (TOP2A) [36], and the focal adhesion adapter protein talin-1 (TLN1) which was recently found to be present also in the nucleus [37]. Immunoblot analysis of the co-IP samples showed that HSF2 interacts with MSH2, SMC2, TOP2A, and TLN1, whereas HSF1 was not found to bind to these proteins (Fig. 1F). This partner specificity between HSF1 and HSF2 is very interesting since it shows that both transcription factors have the potential to operate in distinct protein regulatory networks to achieve unique functions, as suggested before [14,38,39].

The interaction between HSF2 and TLN1 is conserved from mouse to human

Of the novel HSF2-interacting partners, we focused on TLN1 which connects the integrin transmembrane receptors with the actin cytoskeleton at focal adhesions [29]. To investigate the molecular mechanism underlying the HSF2-TLN1 interaction we utilized several mammalian cell lines. We performed co-IP of HSF2 in mouse teratocarcinoma F9 cells, in which the levels of HSF2 are considerably higher compared to other murine cells [40] (Fig. 2A). Immunoblotting showed the formation of HSF2 and HSF1 heterotrimers as well as an association between HSF2 and TLN1. Based on this finding, we asked whether the HSF2-TLN1 interaction is conserved from mouse to human. We first analyzed TLN1, HSF2, and HSF1 levels in different human cell lines, i.e., human prostate epithelial RWPE-1 and human prostate carcinoma PC-3 cells along with murine F9 cells and testis (Fig. 2B). The immunoblotting showed ubiquitous expression of TLN1, HSF2, and HSF1 in all the studied cell lines and testis. Following this, we immunoprecipitated HSF2 from RWPE-1 and PC-3 cells (Fig. 2C). To exclude an unspecific interaction of TLN1 with our HSF2 antibody, we also performed the reciprocal co-IP experiment with a TLN1-specific antibody. The experiments revealed that HSF2 and TLN1 form protein complexes in these human cell lines, confirming that the HSF2-TLN1 interaction is indeed conserved from mouse to human. In contrast, HSF1 and TLN1 were not found in the same protein complex, demonstrating that HSF1-HSF2 heterotrimers do not bind to TLN1 (Fig. 2C).

Prompted by the conserved nature of HSF2-TLN1 interaction, we performed HSF2 co-IP coupled with
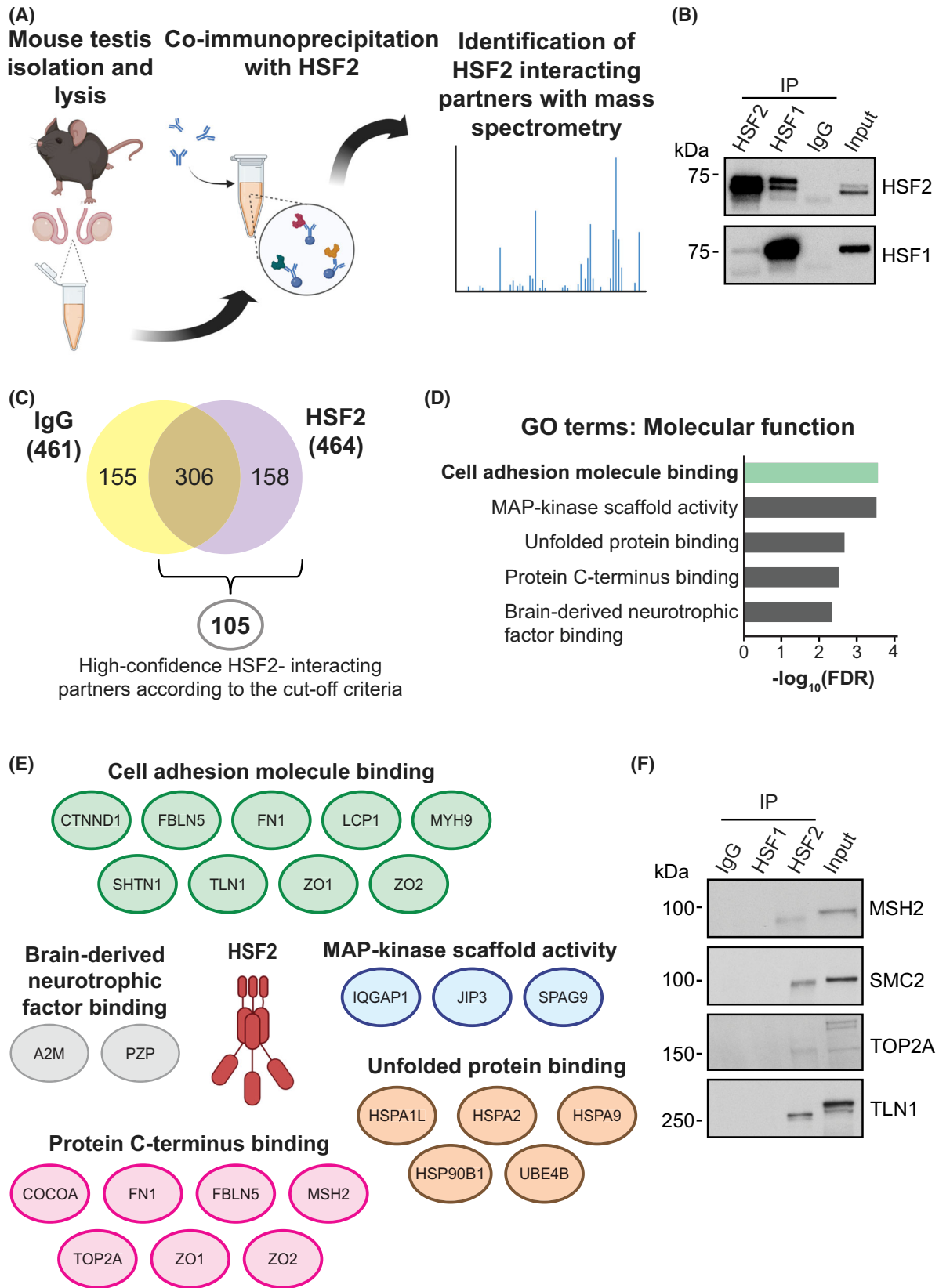
Fig. 1. Identification of the HSF2 interactome in mouse testes. (A) A schematic figure of the workflow. Isolated mouse testes were lysed, and endogenous HSF2 protein was immunoprecipitated with an antibody specific for HSF2. IgG was used as a negative control. The HSF2 co-immunoprecipitated (co-IP) proteins were subsequently identified through liquid chromatography–tandem mass spectrometry (LC–MS/MS). (B) Immunoblot analysis of HSF2 and HSF1 in corresponding co-IP and input samples derived from mouse testes. HSF1 was used as a positive control and IgG as a negative control. The immunoblots are representative figures of two biological replicates run on different gels. (C) Venn diagram showing shared and distinct proteins identified by LC–MS/MS in the HSF2 co-IP sample and the IgG negative control. After applying cut-off criteria (peptide spectrum matches [PSMs] > 2 and a ratio of HSF2 PSMs/IgG PSMs > 3), a total of 105 proteins were identified. (D) Gene ontology (GO) analysis showing terms associated with the 105 HSF2-binding partners. The molecular function GO terms were ranked according to their false discovery rate (FDR) and the redundant terms were withdrawn. The top five GO term categories are shown. (E) HSF2-binding partners within the top five categories shown in D. (F) Immunoblot analysis of MSH2, SMC2, TOP2A, and TLN1 in HSF2 and HSF1 co-IP and input samples derived from mouse testis. IgG was used as a negative control. The immunoblots are representative figures of three biological replicates run on different gels.

LC–MS/MS in PC-3 cells. This analysis identified 113 proteins as binding partners of HSF2, compared to the negative control IgG, with SAINT score ≥ 0.5 (Table S2). By analyzing GO terms associated with HSF2 partners using shinygo [32], we found that cell adhesion molecule binding was the predominant GO term also in the PC-3 cells (Fig. 2D). Intriguingly, several proteins within this GO term category overlapped with those identified as HSF2 partners in mouse testis (Figs 1E and 2E). These included fibronectin [41], the tight junction adapter proteins ZO1 and ZO2 [42], and most importantly, TLN1. This finding provided additional support to continue the investigation of HSF2-TLN1 interaction in PC-3 cells.

To reveal the subcellular localization of the HSF2-TLN1 interaction, and to validate its occurrence in intact cells, we employed proximity ligation assay (PLA) using PC-3 cells. Before conducting the PLA, we investigated the localization of HSF2 and TLN1 in PC-3 cells with indirect immunofluorescence. While HSF2 showed predominantly nuclear localization, TLN1 was mainly detected in the cytoplasm and the vicinity of the plasma membrane (Fig. 3A). The PLA showed that HSF2 and TLN1 are in close proximity (≤ 40 nm) to each other, indicating that these proteins are found in the same complex (Fig. 3B). The negative control composed of two GFP antibodies showed a dramatic reduction in the corresponding signal, confirming the specificity of the PLA results. To explore the subcellular localization of the HSF2-TLN1 interaction, we visualized the PLA images using an orthogonal projection (Fig. 3C). Surprisingly, we observed that the slight majority of the PLA signal was localized within the nucleus, which is in agreement with our recent preprint article reporting nuclear localization of TLN1 [37] (Fig. 3D).

The C-terminus of HSF2 binds directly to TLN1

Since the co-IP assays showed that HSF2, but not HSF1, binds to TLN1, we compared the domain structures of these HSFs. HSF1 and HSF2 are composed of a DNA-binding domain (DBD), an oligomerization domain containing hydrophobic-leucine-zipper-like heptad repeats (HR-A/B), a C-terminal heptad repeat domain (HR-C), regulatory domains (RD), and transactivation domains (AD) (Fig. 4A). Beyond the DBD, HSF1 and HSF2 share approximately 35% identity, which indicates that these proteins are considerably different from each other [23]. Hence, we aligned the amino acid sequences of these HSFs in different species to identify HSF2-specific regions that could potentially bind to TLN1. A sequence alignment of HSF1 and HSF2 from *Homo sapiens*, *Mus musculus*, *Bos taurus*, *Sus scrofa*, *Gallus gallus* and *Danio rerio* unveiled that the longest conserved HSF2-specific sequence is located in its C-terminus (Fig. 4B). Prompted by this finding, we searched for a TLN1-binding motif in the C-terminus of HSF2. Among the best-characterized TLN1-binding motifs is a leucine aspartic acid (LD) motif sequence following the consensus LDXLLXXL [43,44]. Comparison between the HSF2-specific sequence and five known TLN1-interacting proteins that contain an LD motif, i.e. DLC1, RIAM, PXN, KANK1, and KANK2, revealed that the C-terminus of HSF2 indeed contains a putative LD motif (Fig. 4C). TLN1 is composed of an N-terminal FERM domain (also known as the head domain) and a C-terminal flexible rod domain, which are connected through a linker [29]. The head domain of TLN1 consists of four subdomains (F0–F3), whereas the rod domain consists of 13 helical bundles (R1–R13) and a dimerization domain (DD) arranged sequentially like beads on a string [31] (Fig. 4D). Importantly, the TLN1-interacting proteins DLC1, RIAM, PXN, KANK1, and KANK2 bind to either the R7 or R8 helical bundle with their LD domain (Fig. 4D), although RIAM and PXN show greater promiscuity and bind to multiple rod domain.

To test whether HSF2 binds to TLN1 via its putative LD motif, we performed a fluorescent
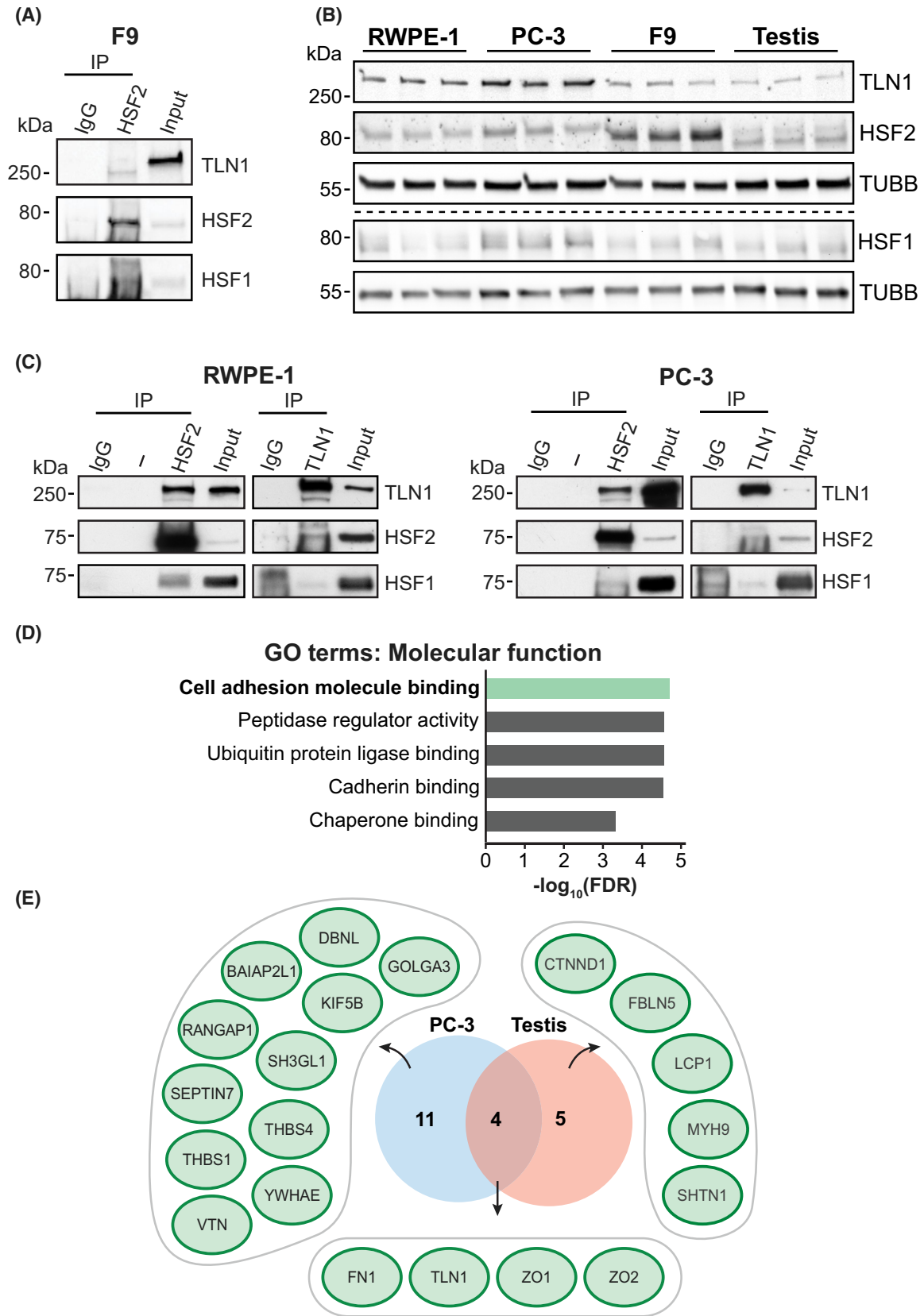
Fig. 2. The HSF2 and TLN1 interaction is conserved from mouse to human. (A) Immunoblot analysis of HSF2 co-IP samples from the mouse cell line F9. HSF1 was used as a positive control for HSF2 co-IP and IgG was used as a negative control. (B) Immunoblot analysis of HSF2, TLN1, and HSF1 expression in three biological replicates from human RWPE-1 and PC-3 cells, mouse F9 cells, and testis. Tubulin (TUBB) was used as a loading control. (C) Immunoblot analysis of HSF2 and TLN1 in corresponding co-IP samples from RWPE-1 and PC-3 cells. HSF1 was used as a positive control for HSF2 co-IP and IgG was used as a negative control. The immunoblots are representative figures of three biological replicates (A, C). (D) The top five molecular function GO terms associated with HSF2 interacting partners in PC-3 cells. HSF2 co-IP samples were analyzed by LC-ESI-MS/MS and IgG was used as a negative control. The GO terms were ranked according to their false discovery rate (FDR) and the redundant terms were withdrawn. (E) A comparison of the HSF2 interacting proteins associated with the GO term cell adhesion molecule binding in PC-3 cells and mouse testis.

polarization assay with a peptide containing the last 16 C-terminal amino acids of HSF2 and protein fragments corresponding to three different regions of the rod domain of TLN1 (R4–R8, R9–R12, R13–DD). As a positive control, we used a peptide containing the LD motif of KANK1 [47]. Our results showed binding between the C-terminus of HSF2 and both the R4-R8 and R9-R12 TLN1 fragments (Fig. 5A). Next, we validated these *in vitro* results in human cells. To this end, we constructed two fusion proteins consisting of monomeric EGFP (mEGFP) coupled with the last 25 C-terminal amino acids of either HSF1 or HSF2: HSF1-c25 and HSF2-c25 (Fig. 5B). PC-3 cells were transfected with mEGFP (Mock), HSF1-c25 or HSF2-c25, and GFP-Trap beads were used for immunoprecipitation of each fusion protein. Immunoblotting of TLN1 revealed that only the HSF2-c25 fusion protein interacts with TLN1 (Fig. 5C), demonstrating that these amino acids of HSF2 are sufficient to mediate the HSF2-TLN1 complex formation. Since the TLN1 immunoblot showed an additional lower band in all the samples, we tested the specificity of our co-IP protocol by downregulating HSF2. For that purpose, PC-3 cells were transfected with either a Scramble or an HSF2-targeting shRNA [48] (Fig. 5D), and the endogenous HSF2 was immunoprecipitated (Fig. 5E). Congruently with the pattern of bands observed in the HSF2-c25 fusion protein co-IP (Fig. 5C), downregulation of HSF2 abolished the upper band (Fig. 5E). Next, we overexpressed the HSF2-c25 fusion protein in PC-3 cells to compete with TLN1 binding to full-length HSF2. We previously showed that HSF2 impacts spheroid formation in the Ultra-Low Attachment (ULA) assay [6], and therefore, we chose to investigate the effect of HSF2-c25 overexpression under similar conditions. Our findings demonstrate that PC-3 cells overexpressing the last 25 amino acids of the HSF2 C-terminus formed less compact spheres occupying significantly larger areas than the Mock-transfected counterparts (Fig. 5F). This implies that the C-terminus of HSF2 has a functional impact on cell adhesion.

Discussion

The protein networks associated with HSF2 have been largely unexplored and only a handful of HSF2-interacting partners have been described in the literature [24–28]. Here, we provide the first proteomic profiling of HSF2 protein partners in a physiologically relevant context. We performed an LC–MS/MS analysis to identify binding proteins of endogenous HSF2 in mouse testes, a tissue where HSF2 is required for proper formation of haploid spermatozoa during spermatogenesis [10,12,14]. The results show that HSF2 interacts with proteins of different molecular functions, among which cell adhesion-related proteins were predominant. This finding was substantiated by mass spectrometry analysis conducted in human prostate carcinoma PC-3 cells. These results are especially interesting because increasing evidence indicates a functional link between HSF2 and cell adhesion. Lack of HSF2 disrupts the expression of a wide variety of cadherin superfamily members, which are cell–cell adhesion receptors crucial for maintaining tissue integrity, and consequently impairs the cell–cell adhesion in human osteosarcoma cells [6,28]. The HSF2-dependent disruption of N-cadherin expression is also linked to neuroepithelial defects in Rubinstein-Taybi syndrome [28]. In contrast, downregulation of HSF2 in PC-3 3D organotypic cell cultures markedly reduced the expression of cell-matrix adhesion proteins (e.g. integrins), extracellular matrix proteins (e.g. collagens), and regulators of cytoskeletal organization (e.g. members of the Rho family of GTPases), leading to increased tumor growth and invasion [33]. These findings collectively suggest that HSF2 regulates both cell-matrix and cell–cell adhesions.

In line with HSF2's adhesion-related function, our proteomic profiling in mouse testis uncovered an interaction between HSF2 and several adapter proteins belonging to major cell-matrix and cell–cell adhesion protein complexes in the vicinity of the plasma membrane, i.e. TLN1, ZO1, ZO2, and CTNND1 [42,49,50]. Through interactions with the cell adhesion adapter
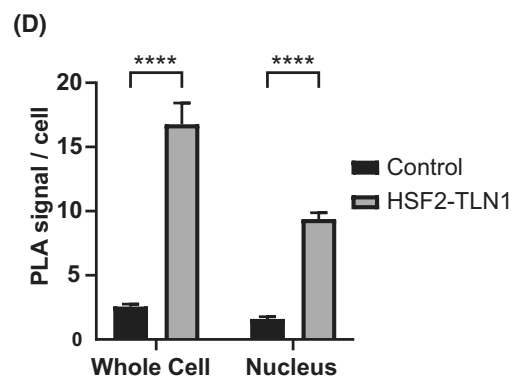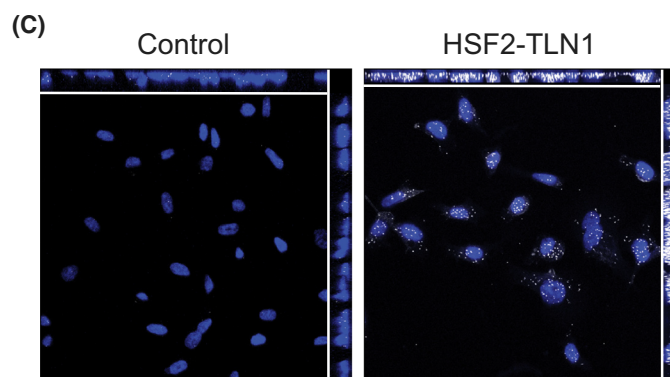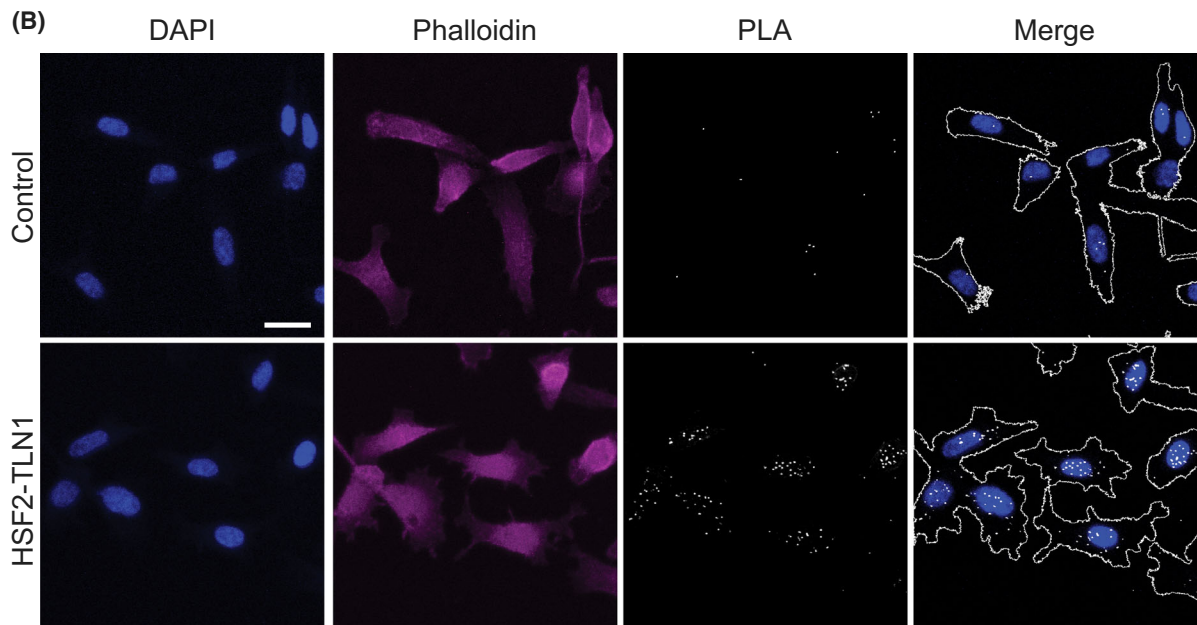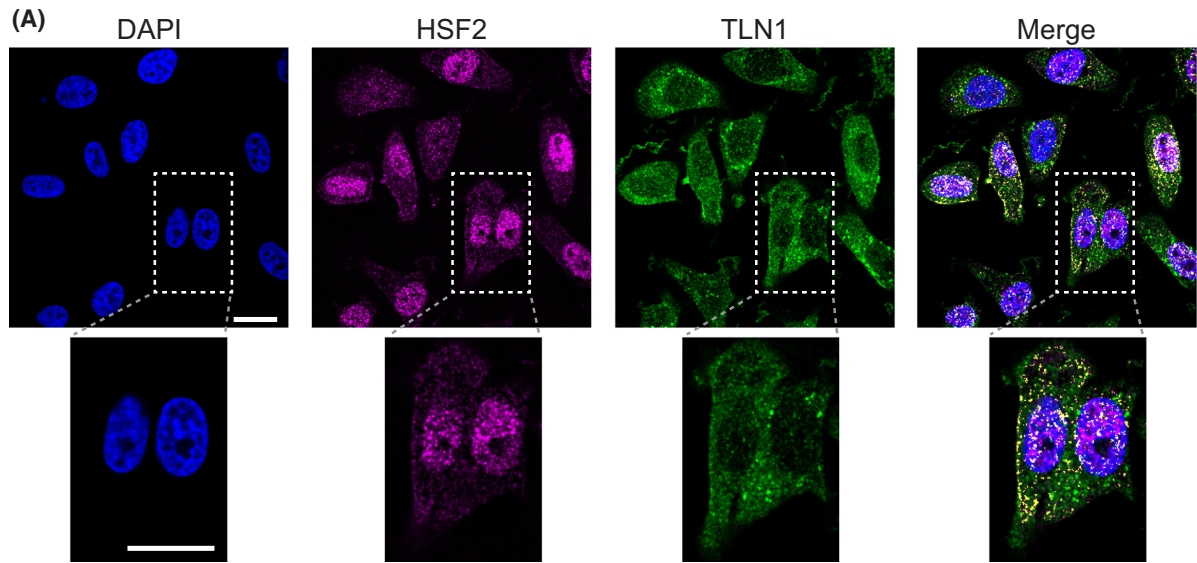
Fig. 3. HSF2 and TLN1 localization and interaction in PC3 cells. (A) Confocal microscopy images with immunofluorescence staining of PC-3 cells showing nuclei (DAPI, blue), HSF2 (magenta), and TLN1 (green). The overlay of the three channels is shown in the merge (yellow) and zoomed-in areas in the lower panels. Images are from a single plane and are representative of three biological replicates. Scale bar 20 µm. (B) Proximity ligation assay (PLA) with antibodies specific for HSF2 and TLN1 in PC-3 cells. As negative controls, antibodies against a non-specific target (GFP) were used. Phalloidin staining (magenta) was used to visualize the borders of the cells, which were marked with white lines in the merge image. The PLA signal appears as white dots indicating close proximity (≤ 40 nm) of the antibodies. Images are shown as maximum intensity projections and they are representative of over 100 cells analyzed per staining. Scale bar 20 µm. (C) Orthogonal projection of a representative PLA image. The PLA signal is depicted as white dots and the nuclei are stained with DAPI (blue). (D) Quantification of the PLA signal in the whole cell and nucleus. A Mann–Whitney *t*-test was performed using GRAPHPAD PRISM 7. The data is presented as mean values of over 100 cells analyzed from across multiple experiments + SEM. ****$P < 0.0001$.

proteins, HSF2 could thus maintain proper cell-matrix and cell–cell contacts needed for normal sperm development. Notably, recent findings have revealed that HSF2 localizes not only within the nucleus and cytoplasm but also at cell adhesion sites on plasma membrane across a wide range of human tissues, suggesting a role in monitoring the integrity of cell adhesion contacts [51].

Based on the previously reported evidence for HSF1 and HSF2 forming heterotrimers in mouse testes [21], we also investigated whether the validated HSF2 partners (Fig. 1F), i.e. TLN1, MSH2, SMC2, and TOP2A, interact with HSF1. Strikingly, HSF1 was not found in complex with any of these novel HSF2-interacting proteins, indicating that HSF2 hetero- and homo-oligomers have distinct protein partners. This finding is particularly important because it demonstrates that although HSF1 and HSF2 share certain functional domains, they also have unique molecular characteristics.

Accordingly, when we explored the differences in protein sequences between HSF1 and HSF2 in *H. sapiens*, *M. musculus*, *B. taurus*, *S. scrofa*, *G. gallus*, and *D. rerio*, we observed a conserved region at the end of the HSF2 C-terminus that is absent from HSF1. The HSF2-specific sequence contains a putative LD TLN1-binding motif, which allowed HSF2 to directly bind to two regions of the TLN1 rod domain (R4–R8 and R9–R12) *in vitro*. This binding pattern is different from other known LD-containing TLN1-binding partners, which only bind to individual helical bundles of TLN1 [44,52], and warrants more detailed structural analysis in forthcoming studies. Moreover, we show that the C-terminal amino acids of HSF2 are sufficient to mediate the formation of the HSF2-TLN1 complex in PC-3 cells and that their overexpression leads to impaired cell adhesion. These findings indicate that the C-terminal region of HSF2 interacts with TLN1 in mammals and that this interaction facilitates formation of cell–cell adhesion. Since HSF2 has been proposed as a central regulator of cadherin genes [6], we suggest that the interaction between HSF2 and TLN1 is essential for HSF2 to effectively modulate the

expression of cell adhesion genes, thereby establishing proper cell–cell contacts. We hypothesize that HSF2 and TLN1, identified as a complex in both the cytoplasm and nucleus in our PLA (Fig. 3D), shuttle to the nucleus to relay signals initiated at cell adhesion sites and adjust gene expression accordingly. This hypothesis is supported by findings of HSF2 localization at cell–cell adhesion sites in various human tissues [51] and recent reports highlighting the interplay between cell-matrix and cell–cell adhesion complexes at adherens junctions and integrin adhesions [53,54]. Through the complex formation capacity with TLN1, HSF2 could thus be a component of the signaling axis that senses changes in cell adhesion. However, future studies are needed to unravel the spatial and temporal dynamics of the HSF2-TLN1 interaction across different cellular compartments, and the signals leading to their complex formation and nuclear translocation.

In this study, we identify the *in vivo* HSF2 interactome in mouse testes and validate novel protein partners of HSF2. We demonstrate that HSF2 exhibits a unique partner specificity compared to HSF1, which is particularly important as it establishes a new layer of functional complexity for HSFs. Indeed, specific protein networks could orchestrate the activation, localization, and function of HSF1 and HSF2 in different biological milieus. Moreover, we identify TLN1 as the first adhesion-related HSF2-interacting partner. We show that the HSF2-TLN1 interaction is conserved from mouse to human, and is mediated by a specific motif in the C-terminus of HSF2. Our results establish a direct molecular link between HSF2 and TLN1, thereby strengthening the association between HSF2 and cellular adhesion processes.
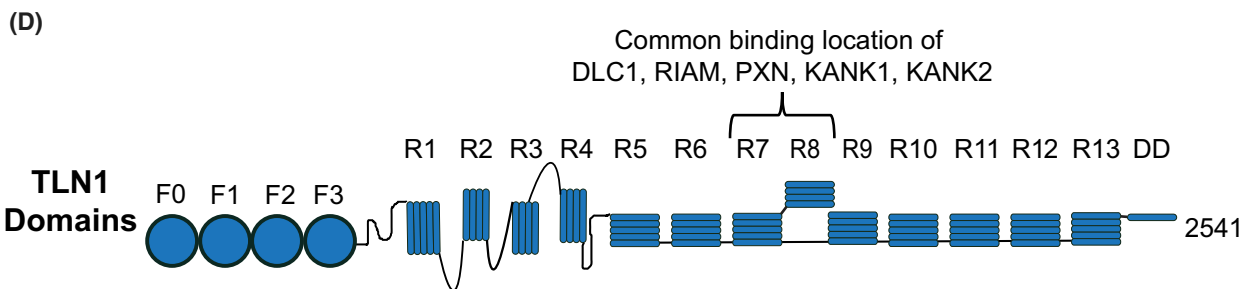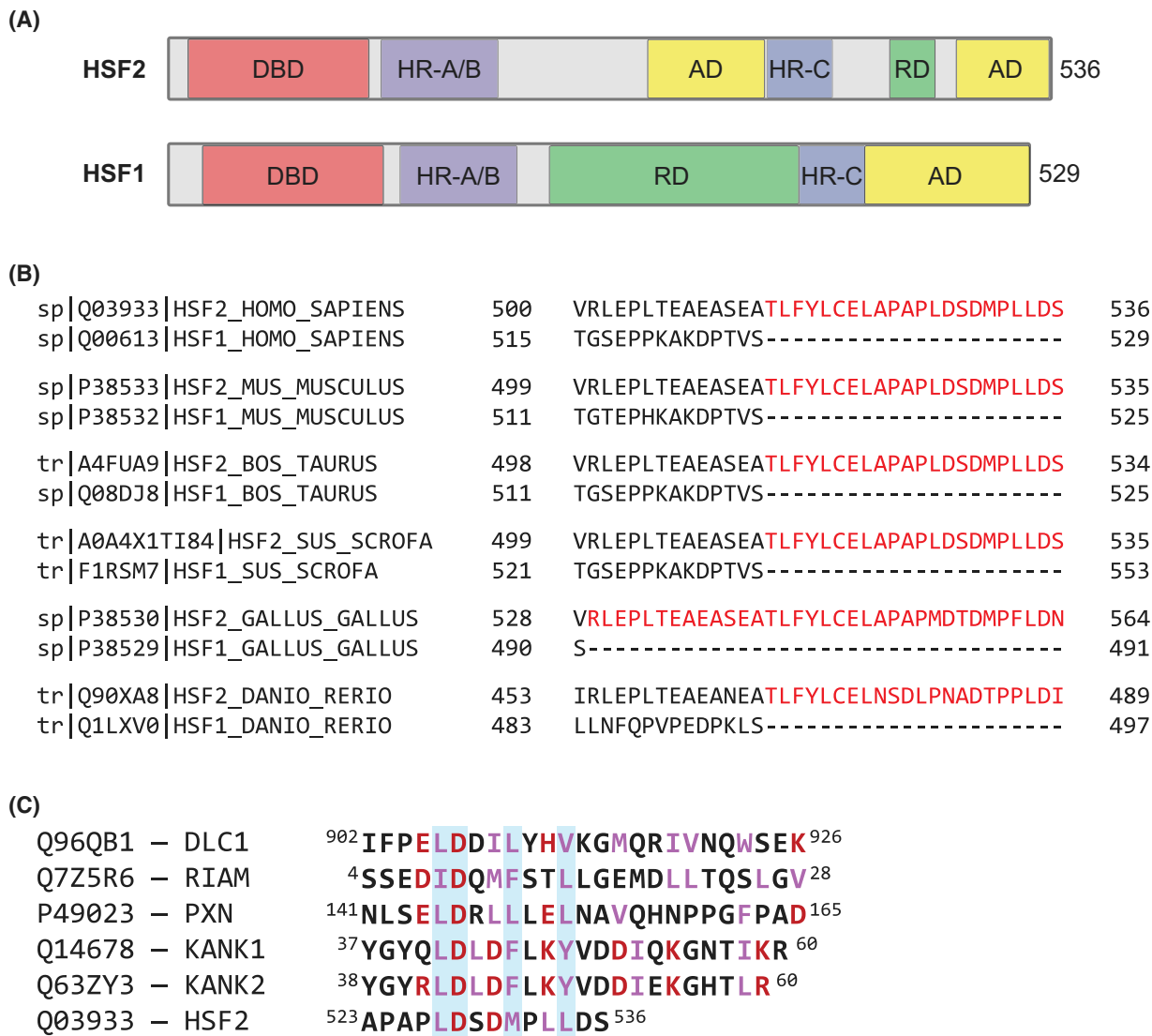
Materials and methods

Mice

Male hybrid mice of the B6129SF2/J strain (the Jackson Laboratory, Bar Harbor, ME, USA) were used for co-immunoprecipitation assays. The pathogen-free mice were

housed under controlled environmental conditions at the Central Animal Laboratory of the University of Turku, Finland. Adult (60–80 days old) mice were sacrificed by CO_2 asphyxiation and cervical dislocation, followed by the isolation of testes, as approved by the Central Animal Laboratory of the University of Turku, Finland (project no. KEK/061002).

Cell culture

All cells were obtained from ATCC (Manassas, VA, USA) and maintained at 37 °C in a humidified 5% CO_2 atmosphere. Mouse teratocarcinoma F9 (RRID:CVCL_0259) cells were cultured in suspension with DMEM (Dulbecco's Modified

(A)

(B)

sp|Q03933|HSF2_HOMO_SAPIENS	500	VRLEPLTEAEASEATLFYLCELAPAPLDSDMPLLDS	536
sp|Q00613|HSF1_HOMO_SAPIENS	515	TGSEPPKAKDPTVS---------------------	529
sp|P38533|HSF2_MUS_MUSCULUS	499	VRLEPLTEAEASEATLFYLCELAPAPLDSDMPLLDS	535
sp|P38532|HSF1_MUS_MUSCULUS	511	TGTEPHKAKDPTVS---------------------	525
tr|A4FUA9|HSF2_BOS_TAURUS	498	VRLEPLTEAEASEATLFYLCELAPAPLDSDMPLLDS	534
sp|Q08DJ8|HSF1_BOS_TAURUS	511	TGSEPPKAKDPTVS---------------------	525
tr|A0A4X1TI84|HSF2_SUS_SCROFA	499	VRLEPLTEAEASEATLFYLCELAPAPLDSDMPLLDS	535
tr|F1RSM7|HSF1_SUS_SCROFA	521	TGSEPPKAKDPTVS---------------------	553
sp|P38530|HSF2_GALLUS_GALLUS	528	VRLEPLTEAEASEATLFYLCELAPAPMDTDMPFLDN	564
sp|P38529|HSF1_GALLUS_GALLUS	490	S----------------------------------	491
tr|Q90XA8|HSF2_DANIO_RERIO	453	IRLEPLTEAEANEATLFYLCELNSDLPNADTPPLDI	489
tr|Q1LXV0|HSF1_DANIO_RERIO	483	LLNFQPVPEDPKLS---------------------	497

(C)

Q96QB1 — DLC1	902 IFPELDDILYHVKGMQRIVNQWSEK	926
Q7Z5R6 — RIAM	4 SSEDIDQMFSTLLGEMDLLTQSLGV	28
P49023 — PXN	141 NLSELDRLLELNAVQHNPPGFPAD	165
Q14678 — KANK1	37 YGYQLDLDFLKYVDDIQKGNTIKR	60
Q63ZY3 — KANK2	38 YGYRLDLDFLKYVDDIEKGHTLR	60
Q03933 — HSF2	523 APAPLDSDMPLLDS	536

(D)

Common binding location of
DLC1, RIAM, PXN, KANK1, KANK2

Fig. 4. The C-terminus of HSF2 is distinct from that of HSF1 and contains a TLN1-binding motif. (A) Schematic figure of human HSF1 and HSF2 domains, modified from [23], which is regulated by a CC-BY-NC-ND 4.0 license (https://creativecommons.org/licenses/by-nc-nd/4.0/). HSF1 and HSF2 have a highly conserved (70% identity) DNA-binding domain (DBD), while the remaining protein sequences show approximately 35% identity. Both HSFs contain an oligomerization domain composed of hydrophobic-leucine-zipper-like heptad repeats (HR-A/B), and C-terminal heptad repeat domain (HR-C), regulatory domains (RD), and transactivation domains (AD). (B) Sequence alignment of HSF2 and HSF1 amino acid sequences in *Homo sapiens*, *Mus musculus*, *Bos taurus*, *Sus scrofa*, *Gallus gallus*, and *Danio rerio*. Sequences obtained from UniProt were aligned with CLUSTAL OMEGA (version 1.2.4), [45,46] and HSF2-specific amino acid sequences are depicted in red. The corresponding UniProt accession numbers are indicated. (C) Multiple sequence alignment of the TLN1-binding LD motifs in known TLN1-binding partners (DLC1, RIAM, PXN, KANK1, KANK2) and HSF2. The key amino acids of the LD motif are aligned across the different proteins in green. Hydrophobic residues are depicted in purple whereas polar hydrophilic residues are in red. Modified from Ref. [47] to include the manual alignment of HSF2 and adapted to use the human amino acid sequences with the indicated UniProt accession numbers. Reference [47] is regulated under the terms of a CC-BY 4.0 Creative Commons Attribution license (https://creativecommons.org/licenses/by/4.0/). (D) Schematic figure of TLN1 domains, modified from [29], which is regulated under the terms of a CC-BY 4.0 Creative Commons Attribution license (https://creativecommons.org/licenses/by/4.0/). TLN1 is composed of 18 domains including an N-terminal head domain with four subdomains (F0–F3), a flexible linker, and a C-terminal rod domain composed of 13 alpha-helical bundles (R1–R13) and a dimerization domain (DD).

Eagle's media, D6171; Sigma-Aldrich, Burlington, MA, USA) supplemented with 10% fetal calf serum, 2 mM L-glutamine, and 100 µg·mL^{-1} penicillin–streptomycin. Human prostate epithelial RWPE-1 (RRID:CVCL_3791) cells were cultured in Keratinocyte SFM media (17005042; Thermo Fisher Scientific, Waltham, MA, USA) supplemented with 25 mg of bovine pituitary extract, 2.5 µg of human recombinant EGF, and 100 µg·mL^{-1} penicillin–streptomycin. Human prostate cancer PC-3 (RRID:CVCL_0035) cells were cultured in RPMI (Roswell Park Memorial Institute, 1640; Sigma-Aldrich) supplemented with 10% fetal calf serum, 2 mM L-glutamine, and 100 U·µg^{-1}·mL^{-1} penicillin–streptomycin. All cells were regularly tested to ensure they were Mycoplasma-free.

Transfections and gene silencing

Transfections were performed using the NEON Transfection System (MPK5000; Thermo Fisher Scientific) according to the manufacturer's instructions unless otherwise specified. Briefly, 1×10^6 PC-3 cells were suspended in 100 µL of resuspension buffer, mixed with 5 µg of DNA, and electroporated using 1×30 ms 1250 V pulses. Transfections to silence HSF2 were performed using a Gene Pulser XCell electroporation system (1652661; Bio-Rad, Hercules, CA, USA). For each transfection, 6×10^6 PC-3 cells were suspended in 400 µL of Opti-MEM (11058-021; Gibco) and subjected to electroporation (230 V, 975 µF) in BTX electroporation cuvettes (45-0126; BTX, Holliston, MA, USA) with 10 µg of HSF2 targeting shRNA and Scrambled shRNA vectors as previously described [48].

## Preparation of cell lysates from mouse testes and cells

Both testes from different mouse individuals were lysed in lysis buffer (25 mM HEPES, pH 8.0, 100 mM NaCl, 5 mM EDTA pH 8.0, 0.5% Triton X-100, 20 mM β-glycerophosphate, 20 mM pNPP, 100 µM Na$_3$VO$_4$, 0.5 mM

DTT, 0.5 mM PMSF, and protease inhibitor cocktail [04693159001; Roche Diagnostics, Mannheim, Germany]). First, the tissue was suspended in lysis buffer and homogenized using an ULTRA-TURRAX T8 homogenizer (IKA Labortechnik, Staufen im Breisgau, Germany). The resulting lysate was incubated on ice for 15 min and centrifuged at 20 000 *g* for 15 min at 4 °C. The supernatant was collected and the protein concentration was measured with the Bradford reagent.

For lysis of cell lines, the corresponding cells were collected in PBS (L0615; BioWest, Nuaillé, France) and lysed in lysis buffer (25 mM HEPES, pH 8.0, 100 mM NaCl, 5 mM EDTA pH 8.0, 0.5% Triton X-100, 20 mM β-glycerophosphate, 20 mM pNPP, 100 µM Na$_3$VO$_4$, 0.5 mM PMSF, and protease inhibitor cocktail [04693159001; Roche Diagnostics]) for 2 h at 4 °C with rotation. Subsequently, the suspension was centrifuged at 20 000 rcf for 10 min at 4 °C, the supernatant was collected, and the protein concentration was determined by BCA assay (23225; Thermo Scientific).

Co-immunoprecipitation

Cell and/or mouse testes lysate containing 700–750 µg total protein was used for each IP, and all centrifugation steps were at 2000 *g* for 2 min at 4 °C unless otherwise specified. Lysates were first pre-cleared with 30 µL protein G sepharose beads (50% slurry; GE Healthcare, Chicago, IL, USA) by 30 min incubation with rotation at 4 °C. After pre-clearing, the lysates were centrifuged, the supernatants were transferred to 1.5 mL microcentrifuge tubes and antibodies were added. The following antibodies were used; 5 µL of anti-HSF2 58f [48], 5 µg anti-TLN1 8D4 (T3287; Sigma-Aldrich), 5 µg normal rabbit IgG (12-370; Millipore, Burlington, MA, USA), 5 µg normal mouse IgG (12-371; Millipore). Samples were incubated with rotation overnight at 4 °C. Next, 30–40 µL of 50% protein G sepharose bead slurry was added, and the samples were incubated an
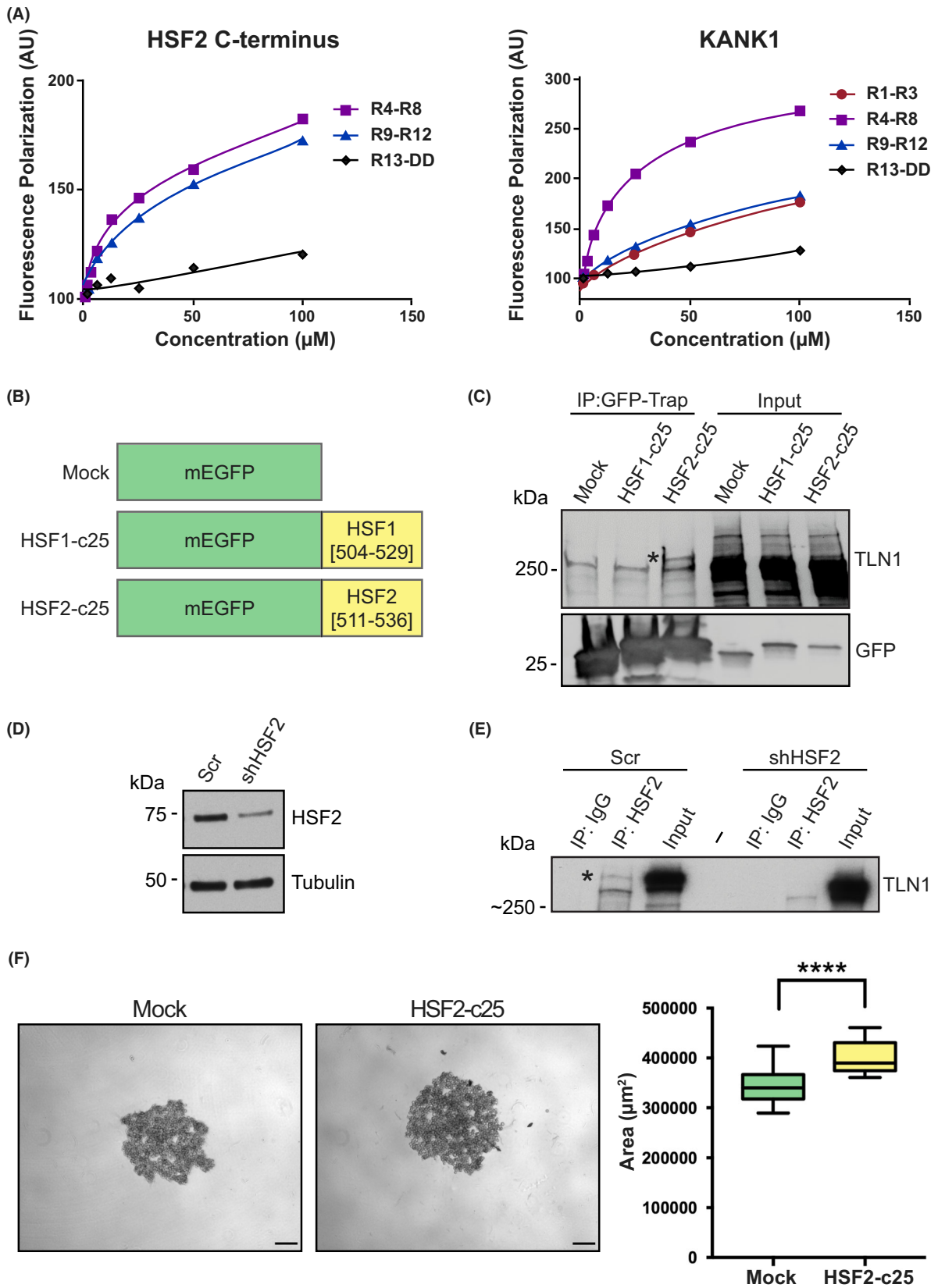
Fig. 5. The C-terminus of HSF2 binds to TLN1. (A) An *in vitro* fluorescent polarization assay between a fluorescently labeled mouse HSF2 peptide containing amino acids 519–535 and three regions of mouse TLN1 (R4–R8, R9–R12, R13–DD). The LD motif of KANK1 was used as a positive control (R1–R3, R4–R8, R9–R12, R13–DD). (B) A schematic overview of fusion proteins containing human HSF1 or HSF2 and monomeric Enhanced Green Fluorescent Protein (mEGFP). The C-terminal amino acids of HSF1 (504–529) and HSF2 (511–536) were fused to mEGFP and named as HSF1-c25 and HSF2-c25. Mock contained only the mEGFP. (C) Immunoblot analysis of TLN1 and GFP in GFP-Trap co-IP and input samples from PC-3 cells expressing Mock, HSF1-c25, or HSF2-c25 constructs. TLN1-HSF2 interaction is indicated with an asterisk. (D) Immunoblot analysis of HSF2 expression in PC-3 cells. PC-3 cells were transfected with scrambled (Scr) or HSF2-targeting shRNA constructs (shHSF2) [48]. Tubulin was used as a loading control. (E) Immunoblot analysis of TLN1 in HSF2 co-IP samples from PC-3 cells. IgG was used as a negative control. The cells were transfected as in (D). TLN1-HSF2 interaction is indicated with an asterisk. The immunoblots in C–E are representative figures of two biological replicates. (F) Representative images of spheroid-like structures in ultra-low attachment plates, scale bar 200 μm (left panel). Quantitative analysis of spheroid area (right panel). The area was quantified in IMAGEJ. Results were plotted as independent data points with mean ± SEM. ****P-value ≤ 0.0001. The data represents three biological replicates.

additional 4 h (at 4 °C, with rotation). Following centrifugation, the supernatant was aspirated, the beads washed four times using 1 mL wash buffer (20 mM Tris–HCl pH 7.5, 1 mM EDTA, 10% glycerol, 150–300 mM NaCl, 0.1% Triton X-100), and 45 μL of 3× Laemmli sample buffer was added to each sample. Input samples were prepared by adding Laemmli sample buffer to 15 μg whole-cell lysate. All samples were boiled for 5 min and centrifuged for 10 min at max speed (21 800 g) at room temperature prior to gel loading.

For GFP-Trap co-IP cell lysate containing 730 μg of total protein was used for each pull-down according to the manufacturer's instructions. Briefly, GFP-Trap beads were washed three times with dilution buffer (25 mM HEPES, pH 8.0, 100 mM NaCl, 5 mM EDTA pH 8.0, 0.5 mM PMSF, and protease inhibitor cocktail [04693159001; Roche Diagnostics]). Cell lysates were adjusted to 500 μL with dilution buffer and incubated with GFP-Trap beads for 1 h at 4 °C with rotation. Next, samples were centrifuged (2500 g for 5 min at 4 °C), the supernatant was aspirated, the beads were washed four times using 0.5 mL wash buffer (20 mM Tris–HCl pH 7.5, 1 mM EDTA, 10% glycerol, 150–300 mM NaCl, 0.1% Triton X-100), and 45 μL of 3× Laemmli sample buffer was added to each sample. Input samples were prepared by adding Laemmli sample buffer to 2.5 μg whole-cell lysate. All samples were boiled for 5 min and centrifuged for 10 min at max speed (21 800 rcf) at room temperature prior to gel loading.

Immunoblotting

Equal amounts of total protein were resolved on 4–20% or 7.5% Mini-PROTEAN® TGX precast gels (Bio-Rad). The proteins were transferred to a nitrocellulose membrane (0.45 μm pore size), which was blocked in 5% milk-PBS with 0.3% Tween 20 for 1 h at room temperature. The primary antibodies were diluted in 0.5% BSA-PBS-0.02% NaN$_3$. 1 : 1000 anti-MSH2 (NA27; Millipore), 1 : 600 anti-SMC2 (D23C5; Cell Signaling Technologies, Danvers, MA, USA), 1 : 1000 anti-TOP2A (4733; Cell Signaling), 1 : 1000 anti-HSF2 (MAB88079; Millipore), 1 : 1000 anti-HSF2

(HPA031455; Sigma-Aldrich), 1 : 1000 anti-HSF1 (RT-629-P1; Neomarkers, Fremont, CA, USA), 1 : 1000 anti-TLN1 8D4 (T3287; Sigma-Aldrich), anti-GFP (632381; Clontech, Mountain View, CA, USA), anti-tubulin (T8328; Sigma-Aldrich). The nitrocellulose membranes were incubated with the primary antibodies overnight at 4 °C. Secondary HRP-conjugated antibodies were purchased from Promega (Madison, WI, USA) or GE Healthcare (anti-mouse, W4021, Promega; anti-rabbit, W4011, Promega; anti-rat, NA935V, GE Healthcare). All secondary antibodies were diluted in 5% milk-PBS with 0.3% Tween 20. The nitrocellulose membranes were incubated with the secondary antibodies at least 1 h at room temperature, and then incubated with enhanced chemiluminescence reagent (28980926, GE Healthcare; 34579, Thermo Scientific; 34094, Thermo Scientific). Images were acquired with an iBright FL1000 or CL1000 imaging system (Thermo Scientific), or a Curix 60 X-ray film processor (Agfa, Mortsel, Belgium).

Experimental design and rationale of mass spectrometry

For the mass spectrometry experiment from mouse testes, the testes from three mice were isolated, lysed as a pool, and 8 mg of protein were used for co-IPs. All centrifugation steps were 2000 rcf for 2 min at 4 °C, unless specified. Protein lysates were first pre-cleared with 100 μL protein G sepharose beads (50% slurry; GE Healthcare) by 30 min incubation with rotation at 4 °C. After centrifugation, the supernatants were transferred to 1.5 mL microcentrifuge tubes and antibodies were added. The following antibodies were used: 50 μL of anti-HSF2 58f [48] and as a negative control 150 μL normal rabbit IgG (SC-2027; Santa Cruz Laboratories, Dallas, TX, USA). Samples were incubated with the corresponding antibody in rotation at room temperature for 30 min. Next, 130 μL of 50% protein G sepharose bead slurry was added, and the samples were incubated an additional 2–3 h (at 4 °C, in rotation). Following centrifugation, the supernatant was aspirated, the beads washed four times using 1 mL wash buffer (20 mM Tris–HCl pH 7.5, 1 mM EDTA, 10% glycerol, 150–300 mM NaCl, 0.1% Triton X-100), and

200 μL Laemmli sample buffer was added to each sample. Input samples were prepared by adding Laemmli sample buffer to 30 μg whole-cell lysate. All samples were boiled for 5 min and centrifuged for 10 min at max speed (21 800 rcf) at room temperature prior to gel loading.

The supernatants obtained from co-IP were loaded into a 8% polyacrylamide gel. After the proteins were resolved, the gel was treated with fixation solution (30% ethanol, 10% acetic acid) for 18 h, followed by washes with 20% ethanol and water on a platform shaker. The gel was exposed to 1.2 mM sodium thiosulfate pentahydrate for exactly 1.5 min and rinsed with water for 20 s. Subsequently, 11.7 mM silver nitrate was used to stain the gel for 30 min on a platform shaker. After the staining step, development solution (0.217 M potassium carbonate, 60.4 μM sodium thiosulfate pentahydrate, 0.07% formaldehyde) was added. When the bands of the gel had reached the desired intensity, the stop solution (2.5% acetic acid, 418.8 mM sodium thiosulfate pentahydrate) was used. The developed gel was washed with water and stored at 4 °C.

Silver-stained protein bands that were present in the HSF2 co-IP and absent from the IgG negative control were subjected to reduction, alkylation, and in-gel tryptic digestion as described previously [55]. The digests were analyzed by nanoflow liquid chromatography–tandem mass spectrometry (LC–MS/MS) using a Q Exactive mass spectrometer coupled to an EASY-nLC 1000 liquid chromatograph (Thermo Scientific). Database search was performed against the SwissProt (*M. musculus*) using MASCOT 2.4 (Matrix Science, London, UK) via PROTEOME DISCOVERER 1.3 (Thermo Scientific). After applying the cut-off criteria (peptide spectrum matches [PSMs] > 2 and a ratio of HSF2 PSMs/IgG PSMs > 3), a total of 105 HSF2-binding partners were identified.

The PC-3 cell mass spectrometry experiment used three biological replicates of cells transiently transfected with a plasmid coding for mEGFP, and collected 48 h posttransfection. The co-IP was performed using 200 μg total protein, and 5 μL anti-HSF2 58f [48] or 3 μg normal rabbit IgG (12-370; Millipore) antibodies, but otherwise proceeded as described in the co-immunoprecipitation section. After the final wash with wash buffer, traces of detergent were removed by four washes with 500 μL Tris (50 mM, pH 8.0).

The samples were dissolved in 8 M urea in 50 mM Tris–HCl, pH 8, reduced with 10 mM D,L-dithiothreitol, and alkylated with 40 mM iodoacetamide. Subsequently, the samples were digested overnight with sequencing-grade modified trypsin (Promega). After digestion, peptide samples were desalted using a Sep-Pak tC18 96-well plate (Waters, Framingham, MA, USA) and evaporated to dryness. Samples were dissolved in 0.1% formic acid, and for DIA analysis equal volumes of the samples were injected and analyzed. Wash runs were performed between each sample to reduce the potential carry-over of peptides. The LC-ESI-MS/MS analysis was performed by the Turku Proteomics Facility (Turku, Finland), largely as described

previously [56]. A nanoflow HPLC system (Easy-nLC1200; Thermo Fisher Scientific) coupled to the Orbitrap Exploris 480 mass spectrometer (Thermo Fisher Scientific) equipped with a nano-electrospray ionization source and FAIMS interface was used with compensation voltages of −40 and −60 V. Peptides were loaded on a trapping column and subsequently separated inline on a 15 cm C18 column (75 μm × 15 cm, ReproSil-Pur 3 μm 120 Å C18-AQ, Dr. Maisch HPLC). The mobile phase consisted of water with 0.1% formic acid (solvent A) or acetonitrile/water (80 : 20 [v/v]) with 0.1% formic acid (solvent B). A 60 min gradient was used to elute peptides (28 min from 5% to 21% solvent B followed by 22 min from 21% to 36% solvent B and in 5 min from 36% to 100% of solvent B, followed by 5 min wash stage with solvent B).

Samples were analyzed by a data-independent acquisition (DIA) LC–MS/MS method. MS data was acquired automatically by using Thermo XCALIBUR 4.6 software (Thermo Fisher Scientific). In a DIA method, a duty cycle contained one full scan (400–1000 m/z) and 30 DIA MS/MS scans covering the mass range 400–1000 with variable width isolation windows. Data was analyzed with FRAGPIPE v.22.0, using the built-in workflow DIA_DIA-Umpire-SpecLib_Quant. The database search was performed with MSFRAGGER v.4.1 [57,58], against the *H. sapiens* proteome downloaded from Uniprot through FRAGPIPE on June 6th 2024 (options: reviewed sequences only, add decoys, add common contaminants). PERCOLATOR v3.6.5 [59] and PROTEINPROPHET (from PHILOSOPHER v5.1.1 [60,61]) were used for filtering and validation of the MSFragger results. The SAINTexpress [62] option in FRAGPIPE was selected to generate input data for CRAPOME 2.0 [63]. CRAPome analysis (organism: *H. sapiens*, experiment type: endogenous pulldown, quantitation type: SPC) was used for calculating the probabilistic SAINT score [64] for HSF2 protein interactions (HSF2_SP), using the SAINT method with user controls (IgG IP samples). The threshold (SAINT score ≥ 0.5) for HSF2 interactors included for GO term analysis was selected based on the SAINT score for the confirmed HSF2 interacting protein HSF1 (SAINT score 0.57).

Gene ontology term analysis

Gene ontology term analyses were performed with the online application SHINYGO [32]. For analysis performed with SHINYGO v.0.76.1 the following parameters were used: false discovery rate (FDR) cut-off: 0.05, number of top pathways to show: 20, and pathway size min: 2 and max: 2000. Species was set to mouse for analysis of the data from mouse testes, and human for data from PC-3 cells.

Confocal microscopy

For confocal microscopy analyses, 8×10^4 PC-3 cells were plated on MatTek plates (P35GC-1.5-14-C; MatTek

Corporation, Ashland, MA, USA) 48 h before imaging. Cells were fixed with 4% paraformaldehyde for 10 min, permeabilized with 0.5% Triton X-100 and 3 mM EDTA in 1× PBS and washed three times with PBS. Cells were blocked with 10% FBS-PBS for at least 1 h at room temperature, and then incubated with the corresponding primary antibody dilution overnight at 4 °C. The following primary antibodies were diluted in 10% FBS-PBS: 1 : 100 anti-TLN1 8D4 (T3287; Sigma-Aldrich), and 1 : 100 anti-HSF2 (HPA031455; Sigma-Aldrich). After primary antibody incubation the samples were washed three times in PBS and incubated with the corresponding secondary antibody at room temperature for 1 h. The following secondary antibodies were diluted 1 : 500 in 10% FBS-PBS and used: goat anti-rabbit Alexa Fluor 488 (A11008; Thermo Fisher Scientific), and donkey anti-mouse Alexa Fluor 555 (A31570; Life Technologies). After secondary antibody incubation, cells were washed in PBS, incubated with 300 nM DAPI diluted in PBS for 5 min, washed again with PBS, and covered with VECTASHIELD (H-1000; Vector Laboratories, Newark, CA, USA) mounting medium. Images were captured with a 3i CSU-W1 spinning disc confocal microscope (Intelligent Imaging Innovations, Denver, CO, USA).

Proximity ligation assay

Proximity ligation assay (PLA) by DUOLINK was performed according to the manufacturer's recommendation with a few modifications. In brief, PC-3 cells seeded on cover slips were fixed with 3% PFA for 20 min at room temperature followed by blocking and permeabilization with 0.3% Triton X-100, 10% FBS in PBS for 15 min. The coverslips were washed with PBS and incubated overnight at 4 °C with 5 μg·mL^{-1} of the primary antibodies anti-TLN1 8D4 (T3287; Sigma-Aldrich), anti-HSF2 (HPA031455; Sigma-Aldrich), anti-GFP mouse (ab1218; Abcam, Cambridge, UK), and anti-GFP rabbit (A-11122; Thermo Scientific), diluted in 10% FBS in PBS. The probes (DUO92002, DUO92004; Sigma-Aldrich), ligation, and amplification (DUO92008; Sigma-Aldrich) reactions were performed according to the manufacturer's recommendations. During the amplification step, 1 : 500 Alexa Fluor™ 647 Phalloidin (A22287; Thermo Scientific) was also added. The samples were mounted in Mowiol with DABCO and kept in darkness until imaging with a Zeiss LSM510 confocal microscope (Zeiss, Oberkochen, Germany) with a 40× objective and a slice distance of 0.7 μm. At least three stacked images were taken per field and over 100 cells were analyzed per PLA reaction pair.

The PLA confocal images were pre-processed, segmented, and analyzed using the CELLPROFILER software [65] to count the amount of PLA signals per cell. In brief, maximum intensity projections of the PLA confocal images were pre-processed by removing background noise and segmented using OTSU thresholding. The segmented PLA signals were analyzed by a Mann–Whitney *t*-test using GRAPHPAD PRISM 7 (GraphPad Software, La Jolla, CA, USA). The data are presented as mean values of over 100 cells analyzed from across multiple experiments + SEM. ****$P < 0.0001$.

Fluorescence polarization assay

Fluorescence polarization was carried out using an HSF2 peptide with an N-terminal cysteine, sequence C-ELAPAPLDSDMPLLDS (GLBiochem, Shanghai, China), as previously described for KANK peptides [47]. Peptide stock solution was composed of PBS, 100 mg·mL^{-1} TCEP and 0.05% Triton X-100. The Thiol reactive BODIPY TMR dye (Thermo Fisher Scientific) was coupled to the terminal cysteine in the HSF2 peptide. Uncoupled dye was removed using gel filtration with a PD-10 column (GE Healthcare). The Fluorescence Polarization assay was performed using a fixed 0.5 μM concentration of peptide and serial dilution of talin-1 R4-R8, R9-R12, and R13–DD protein with a final volume of 100 μL. Fluorescence Polarization measurements were acquired on a BMGLabTech CLARIOstar plate reader (BMGLabTech, Ortenberg, Germany) at room temperature and analyzed using GRAPHPAD PRISM 6.07. K_d values were calculated with a nonlinear curve fitting using a one site total and non-specific binding model.

Plasmid construction

The EGFP in the pEGFP-N1 vector (Clontech) was mutated into monomeric EGFP (mEGFP) by introducing the A206K mutation [66] with the QuikChange II XL Site-Directed Mutagenesis Kit (Agilent, Santa Clara, CA, USA) and the primers listed in (Table S3), following the kit manufacturer's instructions. Next, DNA fragments coding for the final 25 amino acids of HSF2 or HSF1 as well as overhangs homologous to the mEGFP C-terminus were generated. The HSF1 fragment was ordered as a double-stranded GeneStrand (Eurofins Genomics, Ebersberg, Germany), while the HSF2 fragment was generated by PCR using Q5 High-Fidelity DNA Polymerase (NEB, Ipswich, MA, USA) from an HSF2 plasmid as a template [6]. The sequences of the gene strand and the PCR primers are listed in Table S3. The fragments were inserted into the mEGFP plasmid using the In-Fusion HD cloning kit (639650; Takara Bio, Kyoto, Japan) according to the manufacturer's instructions, resulting in the HSF1-c25 and HSF2-c25 constructs.

Ultra-low attachment assay

PC3 cells transiently transfected with plasmids encoding mEGFP or HSF2-c25 were collected 48 h post-transfection. After counting, 2.7×10^3 cells were placed in each well of

a 96-well Ultra-Low Attachment (ULA) plate (#7007; Corning, NY, USA) with a total volume of 200 μL of cell media. Cells were visualized with a Zeiss Axio Vert. A1 microscope (NA 0.4) after 24 h using a 5× objective. All images were analyzed with IMAGEJ software (version: 1.53t) using the BioVoxxel Toolbox plugin v2.6.0 [67]. Briefly, the images were converted from 16 bit to 8 bit, the background was subtracted using a rolling ball radius of 50 pixels. The perimeter of the spheroids was segmented with the thresholding algorithm of IMAGEJ choosing the dark background option, and the extended particle analyzer option of the BioVoxxel Toolbox plugin was run with default settings using the pixel units and output in pixel options. After obtaining the number of pixels for the corresponding spheroid, the area in micrometers was calculated. Statistical analyses were performed with GRAPHPAD PRISM 7 software (GraphPad Software). The statistical significance was analyzed with a two-tailed student's *t*-test.

Acknowledgements

Conflict of interest

The authors declare no conflict of interest.

Author contributions

AJDS, HSEH, BTG, LS, and EH designed the research. AJDS, HSEH, JCL, REG, LML, and EH performed experiments. SYI and LSC-R performed the LC–MS/MS analysis. AJDS, HSEH, JCL, BTG, EH, and LS interpreted the data. AJDS, HSEH, LS, and EH wrote the manuscript with the contribution of all the authors.

Data availability statement

The data is available within the article and the Supporting Information.

References

1 Kmiecik SW & Mayer MP (2022) Molecular mechanisms of heat shock factor 1 regulation. *Trends Biochem Sci* **47**, 218–234.

2 Joutsen J & Sistonen L (2019) Tailoring of proteostasis networks with heat shock factors. *Cold Spring Harb Perspect Biol* **11**, 1–18.

3 Himanen SV, Puustinen MC, Da Silva AJ, Vihervaara A & Sistonen L (2022) HSFs drive transcription of distinct genes and enhancers during oxidative stress and heat shock. *Nucleic Acids Res* **50**, 6102–6115.

4 Vihervaara A, Sergelius C, Vasara J, Blom MAH, Elsing AN, Roos-Mattjus P & Sistonen L (2013) Transcriptional response to stress in the dynamic chromatin environment of cycling and mitotic cells. *Proc Natl Acad Sci USA* **110**, E3388–E3397.

5 Mahat DB, Salamanca HH, Duarte FM, Danko CG & Lis JT (2016) Mammalian heat shock response and mechanisms underlying its genome-wide transcriptional regulation. *Mol Cell* **62**, 63–78.

6 Joutsen J, Da Silva AJ, Luoto JC, Budzynski MA, Nylund AS, de Thonel A, Concordet JP, Mezger V, Sabéran-Djoneidi D, Henriksson E *et al.* (2020) Heat shock factor 2 protects against proteotoxicity by maintaining cell-cell adhesion. *Cell Rep* **30**, 583–597.e6.

7 Lecomte S, Desmots F, Le Masson F, Le Goff P, Michel D, Christians ES & Le Dréan Y (2010) Roles of heat shock factor 1 and 2 in response to proteasome inhibition: consequence on p53 stability. *Oncogene* **29**, 4216–4224.

8 Shinkawa T, Tan K, Fujimoto M, Hayashida N, Yamamoto K, Takaki E, Takii R, Prakasam R, Inouye S, Mezger V *et al.* (2011) Heat shock factor 2 is required for maintaining proteostasis against febrile-range thermal stress and polyglutamine aggregation. *Mol Biol Cell* **22**, 3571–3583.

9 Abane R & Mezger V (2010) Roles of heat shock factors in gametogenesis and development. *FEBS J* **277**, 4150–4172.

10 Sarge KD, Park-Sarge OK, Kirby JD, Mayo KE & Morimoto RI (1994) Expression of heat shock factor 2 in mouse testis: potential role as a regulator of heat-

shock protein gene expression during spermatogenesis. *Biol Reprod* **50**, 1334–1343.

11 Fiorenza MT, Farkas T, Dissing M, Kolding D & Zimarino V (1995) Complex expression of murine heat shock transcription factors. *Nucleic Acids Res* **23**, 467–474.

12 Muhammad T & Li J (2023) Regulation of germline proteostasis by HSF1 and insulin/IGF-1 signaling. *Biochem Soc Trans* **51**, 501–512.

13 Wang G, Zhang J, Moskophidis D & Mivechi NF (2003) Targeted disruption of the heat shock transcription factor (hsf)-2 gene results in increased embryonic lethality, neuronal defects, and reduced spermatogenesis. *Genesis* **36**, 48–61.

14 Åkerfelt M, Henriksson E, Laiho A, Vihervaara A, Rautoma K, Kotaja N & Sistonen L (2008) Promoter ChIP-chip analysis in mouse testis reveals Y chromosome occupancy by HSF2. *Proc Natl Acad Sci USA* **105**, 11224–11229.

15 Wang G, Ying Z, Jin X, Tu N, Zhang Y, Phillips M, Moskophidis D & Mivechi NF (2004) Essential requirement for both hsf1 and hsf2 transcriptional activity in spermatogenesis and male fertility. *Genesis* **38**, 66–80.

16 Korfanty J, Stokowy T, Widlak P, Gogler-Piglowska A, Handschuh L, Podkowiński J, Vydra N, Naumowicz A, Toma-Jonik A & Widlak W (2014) Crosstalk between HSF1 and HSF2 during the heat shock response in mouse testes. *Int J Biochem Cell Biol* **57**, 76–83.

17 Åkerfelt M, Vihervaara A, Laiho A, Conter A, Christians ES, Sistonen L & Henriksson E (2010) Heat shock transcription factor 1 localizes to sex chromatin during meiotic repression. *J Biol Chem* **285**, 34469–34476.

18 Burchfiel ET, Vihervaara A, Guertin MJ, Gomez-Pastor R & Thiele DJ (2021) Comparative interactomes of HSF1 in stress and disease reveal a role for CTCF in HSF1-mediated gene regulation. *J Biol Chem* **296**, 100097.

19 He H, Soncin F, Grammatikakis N, Li Y, Siganou A, Gong J, Brown SA, Kingston RE & Calderwood SK (2003) Elevated expression of heat shock factor (HSF) 2A stimulates HSF1-induced transcription during stress. *J Biol Chem* **278**, 35465–35475.

20 Alastalo T, Hellesuo M, Sandqvist A, Hietakangas V, Kallio M & Sistonen L (2003) Formation of nuclear stress granules involves HSF2 and coincides with the nucleolar localization of Hsp70. *J Cell Sci* **116**, 3557–3570.

21 Sandqvist A, Björk JK, Åkerfelt M, Chitikova Z, Grichine A, Vourc'h C, Jolly C, Salminen TA, Nymalm Y & Sistonen L (2009) Heterotrimerization of heat-shock factors 1 and 2 provides a transcriptional switch in response to distinct stimuli. *Mol Biol Cell* **20**, 1340–1347.

22 Jaeger AM, Pemble CW, Sistonen L & Thiele DJ (2016) Structures of HSF2 reveal mechanisms for differential regulation of human heat-shock factors. *Nat Struct Mol Biol* **23**, 147–154.

23 Roos-Mattjus P & Sistonen L (2022) Interplay between mammalian heat shock factors 1 and 2 in physiology and pathology. *FEBS J* **289**, 7710–7725.

24 Pesonen L, Svartsjö S, Bäck V, de Thonel A, Mezger V, Sabéran-Djoneidi D & Roos-Mattjus P (2021) Gambogic acid and gambogenic acid induce a thiol-dependent heat shock response and disrupt the interaction between HSP90 and HSF1 or HSF2. *Cell Stress Chaperones* **26**, 819–833.

25 Ahlskog JK, Björk JK, Elsing AN, Aspelin C, Kallio M, Roos-Mattjus P & Sistonen L (2010) Anaphase-promoting complex/cyclosome participates in the acute response to protein-damaging stress. *Mol Cell Biol* **30**, 5608–5620.

26 Xing H, Hong Y & Sarge KD (2010) PEST sequences mediate heat shock factor 2 turnover by interacting with the Cul3 subunit of the Cul3-RING ubiquitin ligase. *Cell Stress Chaperones* **15**, 301–308.

27 Goodson ML, Hong Y, Rogers R, Matunis MJ, Park-Sargell OK & Sarge KD (2001) SUMO-1 modification regulates the DNA binding activity of heat shock transcription factor 2, a promyelocytic leukemia nuclear body associated transcription factor. *J Biol Chem* **276**, 18513–18518.

28 de Thonel A, Ahlskog JK, Daupin K, Dubreuil V, Berthelet J, Chaput C, Pires G, Leonetti C, Abane R, Barris LC *et al.* (2022) CBP-HSF2 structural and functional interplay in Rubinstein-Taybi neurodevelopmental disorder. *Nat Commun* **13**, 7002.

29 Gough RE & Goult BT (2018) The tale of two talins – two isoforms to fine-tune integrin signalling. *FEBS Lett* **592**, 2108–2125.

30 Klapholz B & Brown NH (2017) Talin – the master of integrin adhesions. *J Cell Sci* **130**, 2435–2446.

31 Goult BT, Brown NH & Schwartz MA (2021) Talin in mechanotransduction and mechanomemory at a glance. *J Cell Sci* **134**, 1–7.

32 Ge SX, Jung D, Jung D & Yao R (2020) ShinyGO: a graphical gene-set enrichment tool for animals and plants. *Bioinformatics* **36**, 2628–2629.

33 Björk JK, Åkerfelt M, Joutsen J, Puustinen MC, Cheng F, Sistonen L & Nees M (2016) Heat-shock factor 2 is a suppressor of prostate cancer invasion. *Oncogene* **35**, 1770–1784.

34 Goellner EM (2020) Chromatin remodeling and mismatch repair: access and excision. *DNA Repair (Amst)* **85**, 102733.

35 Skibbens RV (2019) Condensins and cohesins – one of these things is not like the other! *J Cell Sci* **132**, 220491.

36 Uusküla-Reimand L & Wilson MD (2022) Untangling the roles of TOP2A and TOP2B in transcription and cancer. *Sci Adv* **8**, 23–27.

37 da Silva AJ, Hästbacka HSE, Puustinen MC, Pessa JC, Goult BT, Jacquemet G, Henriksson E & Sistonen L (2022) A subpopulation of Talin 1 resides in the nucleus and regulates gene expression. *bioRxiv*. doi: 10.1101/2022.03.15.484419 [PREPRINT].

38 Åkerfelt M, Morimoto RI & Sistonen L (2010) Heat shock factors: integrators of cell stress, development and lifespan. *Nat Rev Mol Cell Biol* **11**, 545–555.

39 Glastad KM, Roessler J, Gospocic J, Bonasio R & Berger SL (2023) Long ant life span is maintained by a unique heat shock factor. *Genes Dev* **37**, 398–417.

40 Murphy SP, Gorzowski JJ, Sarge KD & Phillips B (1994) Characterization of constitutive HSF2 DNA-binding activity in mouse embryonal carcinoma cells. *Mol Cell Biol* **14**, 5309–5317.

41 Spada S, Tocci A, Di Modugno F & Nisticò P (2021) Fibronectin as a multiregulatory molecule crucial in tumor matrisome: from structural and functional features to clinical practice in oncology. *J Exp Clin Cancer Res* **40**, 102.

42 Zihni C, Mills C, Matter K & Balda MS (2016) Tight junctions: from simple barriers to multifunctional molecular gates. *Nat Rev Mol Cell Biol* **17**, 564–580.

43 Tumbarello DA, Brown MC & Turner CE (2002) The paxillin LD motifs. *FEBS Lett* **513**, 114–118.

44 Zacharchenko T, Qian X, Goult BTT, Jethwa D, Almeida TBB, Ballestrem C, Critchley DRR, Lowy DRR & Barsukov ILL (2016) LD motif recognition by Talin: structure of the Talin-DLC1 complex. *Structure* **24**, 1130–1141.

45 Goujon M, McWilliam H, Li W, Valentin F, Squizzato S, Paern J & Lopez R (2010) A new bioinformatics analysis tools framework at EMBL-EBI. *Nucleic Acids Res* **38**, 695–699.

46 Sievers F, Wilm A, Dineen D, Gibson TJ, Karplus K, Li W, Lopez R, McWilliam H, Remmert M, Söding J, Thompson JD & Higgins DG (2011) Fast, scalable generation of high-quality protein multiple sequence alignments using Clustal Omega. *Mol Syst Biol* **7**, 539.

47 Bouchet BP, Gough RE, Ammon YC, van de Willige D, Post H, Jacquemet G, Maarten Altelaar AF, Heck AJ, Goult BT & Akhmanova A (2016) Talin-KANK1 interaction controls the recruitment of cortical microtubule stabilizing complexes to focal adhesions. *Elife* **5**, 1–23.

48 Östling P, Björk JK, Roos-Mattjus P, Mezger V & Sistonen L (2007) Heat shock factor 2 (HSF2) contributes to inducible expression of hsp genes through interplay with HSF1. *J Biol Chem* **282**, 7077–7086.

49 Goult BT, Yan J & Schwartz MA (2018) Talin as a mechanosensitive signaling hub. *J Cell Biol* **217**, 3776–3784.

50 Mège RM & Ishiyama N (2017) Integration of cadherin adhesion and cytoskeleton at adherens junctions. *Cold Spring Harb Perspect Biol* **9**, a028738.

51 Joutsen J, Pessa JC, Jokelainen O, Sironen R, Hartikainen JM & Sistonen L (2024) Comprehensive analysis of human tissues reveals unique expression and localization patterns of HSF1 and HSF2. *Cell Stress Chaperones* **29**, 235–271.

52 Gough RE, Jones MC, Zacharchenko T, Le S, Yu M, Jacquemet G, Muench SP, Yan J, Humphries JD, Jørgensen C *et al.* (2021) Talin mechanosensitivity is modulated by a direct interaction with cyclin-dependent kinase-1. *J Biol Chem* **297**, 1–18.

53 Hadjisavva R, Anastasiou O, Ioannou PS, Zheltkova M & Skourides PA (2022) Adherens junctions stimulate and spatially guide integrin activation and extracellular matrix deposition. *Cell Rep* **40**, 111091.

54 Pulous FE, Grimsley-Myers CM, Kansal S, Kowalczyk AP & Petrich BG (2019) Talin-dependent integrin activation regulates VE-cadherin localization and endothelial cell barrier function. *Circ Res* **124**, 891–903.

55 Imanishi SY, Kochin V, Ferraris SE, de Thonel A, Pallari HM, Corthals GL & Eriksson JE (2007) Reference-facilitated phosphoproteomics: fast and reliable phosphopeptide validation by µLC-ESI-Q-TOF MS/MS. *Mol Cell Proteomics* **6**, 1380–1391.

56 Pavic K, Gupta N, Omella JD, Derua R, Aakula A, Huhtaniemi R, Määttä JA, Höfflin N, Okkeri J, Wang Z *et al.* (2023) Structural mechanism for inhibition of PP2A-B56α and oncogenicity by CIP2A. *Nat Commun* **14**, 1143.

57 Kong AT, Leprevost FV, Avtonomov DM, Mellacheruvu D & Nesvizhskii AI (2017) MSFragger: ultrafast and comprehensive peptide identification in mass spectrometry–based proteomics. *Nat Methods* **14**, 513–520.

58 Teo GC, Polasky DA, Yu F & Nesvizhskii AI (2021) Fast deisotoping algorithm and its implementation in the MSFragger search engine. *J Proteome Res* **20**, 498–505.

59 Käll L, Canterbury JD, Weston J, Noble WS & MacCoss MJ (2007) Semi-supervised learning for peptide identification from shotgun proteomics datasets. *Nat Methods* **4**, 923–925.

60 da Veiga Leprevost F, Haynes SE, Avtonomov DM, Chang H-Y, Shanmugam AK, Mellacheruvu D, Kong AT & Nesvizhskii AI (2020) Philosopher: a versatile toolkit for shotgun proteomics data analysis. *Nat Methods* **17**, 869–870.

61 Nesvizhskii AI, Keller A, Kolker E & Aebersold R (2003) A statistical model for identifying proteins by tandem mass spectrometry. *Anal Chem* **75**, 4646–4658.

62 Teo G, Liu G, Zhang J, Nesvizhskii AI, Gingras A-C & Choi H (2014) SAINTexpress: improvements and additional features in significance analysis of INTeractome software. *J Proteomics* **100**, 37–43.

63 Mellacheruvu D, Wright Z, Couzens AL, Lambert J-P, St-Denis NA, Li T, Miteva YV, Hauri S, Sardiu ME, Low TY *et al.* (2013) The CRAPome: a contaminant repository for affinity purification–mass spectrometry data. *Nat Methods* **10**, 730–736.

64 Choi H, Larsen B, Lin Z-Y, Breitkreutz A, Mellacheruvu D, Fermin D, Qin ZS, Tyers M, Gingras A-C & Nesvizhskii AI (2011) SAINT: probabilistic scoring of affinity purification–mass spectrometry data. *Nat Methods* **8**, 70–73.

65 Carpenter AE, Jones TR, Lamprecht MR, Clarke C, Kang IH, Friman O, Guertin DA, Chang JH, Lindquist RA, Moffat J *et al.* (2006) CellProfiler: image analysis software for identifying and quantifying cell phenotypes. *Genome Biol* **7**, R100.

66 Zacharias DA, Violin JD, Newton AC & Tsien RY (2002) Partitioning of lipid-modified monomeric GFPs into membrane microdomains of live cells. *Science* **296**, 913–916.

67 Brocher J (2023) biovoxxel/BioVoxxel-Toolbox: BioVoxxel Toolbox v2.6.0. *Zenodo*.

Supporting information

Additional supporting information may be found online in the Supporting Information section at the end of the article.

Table S1. Extended mass spectrometry analysis results from mouse testis.

Table S2. Extended mass spectrometry analysis results from human PC-3 cells.

Table S3. Sequences for oligonucleotides used for plasmid construction.